https://doi.org/10.5194/egusphere-2026-5049
Preprint. Discussion started: 11 September 2026

Radiative-dynamical interaction of tropical upper tropospheric clouds: sensitivity to ice cloud parameterizations

Claudia J. Stubenrauch[1], Xiaoting Chen[1], Laurent Li[1], Anthony J. Baran[2,3]

[1]Laboratoire de Météorologie Dynamique / Institut Pierre-Simon Laplace, (LMD/IPSL), CNRS, Sorbonne University, 75005 Paris, France
[2] Met Office, Exeter, UK
[3]School of Physics, Astronomy, and Mathematics, University of Hertfordshire, Hatfield, AL10 9AB, UK

Correspondence: Xiaoting Chen (xiaoting.chen@lmd.ipsl.fr), Claudia J. Stubenrauch (claudia.stubenrauch@lmd.ipsl.fr)

Abstract. Atmospheric heating gradients caused by upper tropospheric (UT) clouds, most abundant in the tropics, influence the atmospheric circulation which then affects patterns of precipitation. We use climate simulations to investigate how the radiative heating from UT clouds affects the large-scale circulation and how the circulation, in turn, influences precipitation. First, we present new observational metrics derived from satellite observations to demonstrate how much the simulated UT cloud properties (ice water path and radiative heating rates) depend on the parameterizations of UT cloud ice and microphysics (single-scattering properties and fall speed). We then examine the consequences of UT cloud – radiation interactions on the Hadley circulation by performing two sets of experiments with UT clouds transparent to radiation, differentiating between semi-transparent and opaque UT clouds. Using ensemble simulations, we are also able to separate immediate effects and feedbacks which build up subsequently. The distribution of UT clouds with respect to their optical depth is key in the sign of the dynamical effect: Semi-transparent cirrus weaken the Hadley circulation by decreasing the meridional heating gradients, whereas opaque UT clouds strengthen the circulation by concentrating radiative heating in the core of the Intertropical Convergence Zone. Furthermore, the radiative heating of the opaque UT clouds is strong enough to considerably affect the precipitation through changes in moisture convergence which itself has been changed by the Hadley circulation.

1 Introduction

Covering about 30% of the Earth (e. g. Stubenrauch et al. 2024), upper tropospheric clouds play a vital role in modulating the Earth's energy budget and heat transport. These clouds, most abundant in the tropics, form either as cirrus anvils from outflow of deep convection or as cirrus by in situ freezing. Cloud processes fundamentally control how feedbacks take place: Climate warming will change tropical convection, which then alters the upper tropospheric (UT) cloud systems, strongly impacting the atmospheric heating. Changes in atmospheric heating gradients influence the atmospheric circulation which then affects the patterns of precipitation.

We have used climate simulations to reply to the following question: How does the radiative heating from UT cloud systems affect the large-scale circulation and how in turn does the circulation influence convection and precipitation?

https://doi.org/10.5194/egusphere-2026-5049
Preprint. Discussion started: 11 September 2026

When convection changes due to climate warming, cloud structure and amount will respond. This then alters the Earth energy balance, causing an additional change of surface temperature. Experiments with climate models suggest that these feedbacks lead to a narrower but more intense latitudinal precipitation band and larger regions with a dry free troposphere (e. g. Mauritsen and Stevens, 2015). Idealized climate experiments traced the cirrus anvil rise and their horizontal shrinking to the dependence of static stability on temperature and pressure (Bony et al., 2016), while a climate feedback process study (Gehlot and Quaas, 2012) suggests a prolonged lifetime and a larger amount of clouds from convection in a warmer climate.

The dynamical response of the climate system to the atmospheric heating induced by UT clouds can only be quantified by large-scale modelling. The importance of this feedback connection has long been demonstrated (e. g. Slingo and Slingo, 1991, Lohmann and Roeckner, 1995; Bergman and Hendon, 2000) in accelerating the jet streams or strengthening the Hadley and Walker circulations. Moreover, Byrne and Schneider (2018) have shown that the equilibrium climate sensitivity (ECS, which describes how much the Earth will warm for a given emission of CO_2) itself depends on the atmospheric circulation response to the radiative forcing at the top of the atmosphere (TOA), particularly in the tropics. More recently, Haslehner et al. (2024) have shown that the radiative interactions of UT clouds warm the entire troposphere, and in particular the upper troposphere, and dominate the overall cloud impact responsible for a reduction in tropical precipitation.

The outcome of such feedback studies relies upon the representation of convection and detrainment as well as of ice optical properties in these models. Del Genio et al. (2005) have revealed that the ECS of climate models depends on how much the parameterized precipitation and detrainment efficiencies increase with surface temperature, as they offset each other in regulating the TOA energy balance. Entrainment, slowing down the convective updraft, has been identified as another factor influencing ECS (Zhao, 2014).

In this article, we utilize the LMDZ climate model (Madeleine et al., 2020) and first assess the sensitivity of the simulated climate to parameterizations of ice cloud microphysics, including single-scattering properties and fall speed, besides the representation of high cloud cover, which is closely linked to the grid cell variability of UT cloud water. We compare UT cloud cover, ice water path and radiative heating rates with distributions of these variables derived from satellite observations. The interaction between clouds and radiation, named as atmospheric cloud radiative effect (ACRE), is a strong modulator of the global energy budget. Assessing the impacts of that interaction provides valuable insights into both present-day climate and future projections.

After having chosen parameterizations which lead to the most realistic high cloud cover, ice water path distributions and radiative heating rates, we study the dynamical effect induced by the interaction between radiation and 1) semi-transparent UT clouds (cirrus) with IWP < 100 gm^{-2} and 2) all UT clouds. While these cirrus clouds have been identified to warm the TOA, the opaque UT clouds have a cooling effect at the TOA (e. g. Sokol et al., 2024).

By performing two sets of experiments, once making only semi-transparent UT clouds transparent to radiation and once making all UT clouds transparent to radiation, we are able to distinguish on one hand the large-scale radiative effect on atmospheric circulation and on the other hand the radiative effect together with the resulting convective coupling. While semi-transparent UT clouds are expected to only affect the atmospheric circulation via their radiative impact, the radiative effect of

https://doi.org/10.5194/egusphere-2026-5049
Preprint. Discussion started: 11 September 2026

opaque UT clouds, including convective towers and thick anvils, is also expected to balance the latent heating and therefore precipitation.

This article is structured in the following way: Section 2 describes the changes which have been applied to parameterizations concerning the modelling of large-scale UT clouds in the LMDZ climate model. Section 3 presents an evaluation of the LMDZ present-day climate simulations using different satellite observations. In Sect. 4, we study the radiative impact of UT clouds, distinguishing between semi-transparent and opaque, on the intensity of the Hadley cell and precipitation. Conclusions are presented in Sect. 5.

2 Changes in UT cloud parameterizations of the LMDZ model

We start from the LMDZ atmospheric general circulation model version, which has been used in CMIP6 (Climate Model Intercomparison Project for the 6th Assessment Report of the Intergovernmental Panel on Climate Change) and which is detailed by Madeleine et al. (2020).

Since we are interested in the effect of large-scale UT cloud radiative effects, we have paid particular attention to the parameterizations of bulk ice crystal single-scattering properties, used in the radiative transfer, large-scale cloud formation and bulk ice crystal fall speed.

2.1 Bulk ice crystal single-scattering properties used in the radiative transfer

Radiative transfer in this version of the LMDZ model is based on the Rapid Radiative Transfer Model (RRTM; Mlawer et al., 1997), with 6 wavelength bands in the SW domain and 16 bands in the LW domain.

Per atmospheric layer and radiative band, the cloud optical depth, τ, necessary for the computation of the radiative fluxes in RRTM, is computed as the product of mass extinction coefficient, k_{ext}^{ice}, (per unit mass of ice, in m^2g^{-1}) and ice water path, IWP. The parameterization of Ebert and Curry (1992; EC) assumes hexagonal ice crystals and expresses k_{ext}^{ice}, the single-scattering albedo, ω_0, and the asymmetry factor, g, for each of the spectral bands as functions of the effective ice crystal radius, r_e. The latter increases linearly with the layer temperature, T, (Iacobellis and Somerville, 2000). In the LW flux computation, scattering is not considered and hence $\tau(\lambda, p) = 1.66 * k_{abs}^{ice}(\lambda, p) * IWP(p)$, where k_{abs}^{ice} is the mass absorption coefficient per unit mass of ice.

We have replaced this parameterization by the one of Baran et al. (2016), which is based on single-scattering properties computed from an ensemble model of cirrus ice crystals, with their habit depending on their size, from hexagonal columns and bullet rosettes towards more complex columnar aggregates (Baran et al., 2014). Baran et al. (2016), then parameterized these single-scattering properties directly as functions of the ice mass mixing ratio, q_{ice}, given as ice mass per unit volume divided by the mass of cloudy air per unit volume or ice water content, IWC, divided by air density (in kg/kg) and T, avoiding the introduction of r_e. However, it is the mass extinction coefficient per unit mass of cloudy air, k_{ext}^{air}, which depends on q_{ice} and T, with $k_{ext}^{ice} = k_{ext}^{air}/q_{ice}$. For the integration into the LMDZ code, we have chosen the coefficients of the spectral bands of the

https://doi.org/10.5194/egusphere-2026-5049
Preprint. Discussion started: 11 September 2026

MetOffice GCM (for details of spectral bands and their widths see Baran et al., 2016) which are the closest (and very similar) to the ones of the LMDZ GCM and use k_{ext}^{ice}.

Furthermore, for the computation of the LW fluxes, we have corrected the cloud optical depth for scattering effects by first taking out the forward peak contribution (estimated as $f = g^2$) from k_{ext}, ω_0 and g, using the δ-function adjustment, and then using these scaled variables to recompute the diffusion / two-stream effective optical depth (Joseph et al., 1976; Stephens, 1984). The formulas are given in Appendix A.

2.2 Large-scale cloud formation

In the LMDZ model, outside grid cells where shallow convection is active, the large-scale cloud cover, α_c^{lsc}, and in-cloud condensed water, $q_c^{in,lsc}$, are computed using a generalized lognormal Probability Density Function (PDF), with a standard deviation σ proportional to the total water within the grid cell, q_t (Madeleine et al., 2020). The relative variability of total water within the grid cell, ξ, is then $\xi = \sigma/q_t$. At present, ξ increases from bottom to top of the atmosphere: It is set close to 0 for p > 600 hPa, while in the upper troposphere, ξ_{UT} is constant and can be tuned.

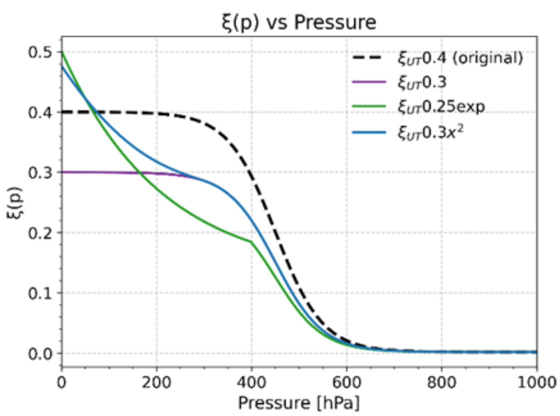

Figure 1: ξ (p) profile of the original LMDZ model (with ξ_{UT} = 0.4 for UT clouds with p < 300hPa) and different modifications. ξ is used to scale the standard deviation σ of the large-scale cloud PDF, with $\sigma = \xi q_t$.

The cloud cover depends on this width as well as on the value of the specific humidity at saturation, q_{sat}, computed as the integral of the specific humidity distribution from q_{sat} onwards. The in-cloud condensed water content is then the ratio of grid-cell averaged condensed water, q_c^{lsc}, and cloud cover: $q_c^{in,lsc} = q_c^{lsc} / \alpha_c^{lsc}$, with q_c being composed of q_{liq} and q_{ice}, according to the layer temperature. The fraction of liquid water is given by Eq. (13) and Fig. 3 of Madeleine et al. (2020). In general, a larger ξ leads to a smaller cloud cover and a larger in-cloud IWP.

In the original LMDZ version, ξ_{UT} is set to 0.4. The p-dependent change between lower and upper troposphere is given as a *tanh* function. Since the current formulation of ξ_{UT} leads to an UT cloud cover which is too small and an in-cloud IWP which is too large, compared to satellite observations (see Sect. 3), we have built different formulations of ξ_{UT}: First, we have changed

https://doi.org/10.5194/egusphere-2026-5049
Preprint. Discussion started: 11 September 2026

ξ_{UT} to a constant 0.3, and then changed $\xi_{UT}(p)$ in such a way that it increases with height, once exponentially and once quadratically. Figure 1 resumes these different formulations of ξ (p).

2.3 Bulk ice crystal fall speed

The current version of the LMDZ model uses a parameterization of Heymsfield and Donner (1990), which estimates the fall speed, v_m, as a function of IWC only. Furthermore, this parameter is multiplied by a scaling factor of 0.8, which has been tuned to achieve radiative balance at TOA.

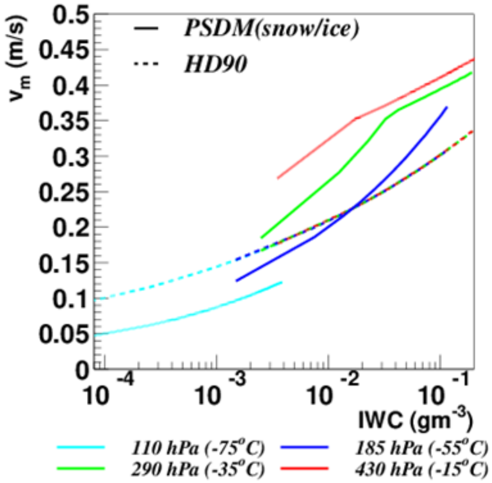

Figure 2: Fall speed as a function of IWC, scaled by a factor 0.8, as used in the LMDZ model, according to the parameterization of Heymsfield and Donner (1990) and to a Particle Size Distribution Moment parameterization, based on Field et al. (2007), using different coefficients for snow and ice.

Meanwhile, many airborne field campaigns and ground based radar measurements have shown that the fall speed not only depends on IWC but also on T (e. g. Deng and Mace, 2008; Mitchell et al., 2011). In order to be more coherent with the ensemble ice crystal model used in the radiative transfer (Sect. 2.1), we have implemented a parameterization based on the ice Particle Size Distribution (PSD) itself. The Particle Size Distribution Moment (PSDM) parameterization of Field et al. (2007) assumes an average T dependence, without distinguishing cirrus types and therefore formation processes, but differences are introduced by linking all moments of the PSD to the IWC (Stubenrauch et al., 2019; Equations S17-S23). The bulk fall speed v_m is determined from the terminal fall velocity v_t of a single ice or snow crystal by integration over the PSD. The mass and the terminal fall velocity are often expressed as a power law of the ice crystal diameter, D: $m = a * D^b$ and $v_t = e * D^f$. We have used two sets of coefficients (a, b, e, f), one for ice and one for snow, and the complete PSDM parameterization of v_m is given by the equations S45 – S50 in the supplement of Stubenrauch et al. (2019).

https://doi.org/10.5194/egusphere-2026-5049
Preprint. Discussion started: 11 September 2026

From Fig. 2, we deduce that the additional T dependence reduces the slope of the v_m - IWC relationship for a given T. Furthermore, it allows v_m to differ in cirrus with the same IWC according to T-dependent changes in ice crystal sizes and habits, leading to a larger v_m at larger T.

3 Evaluation of ice cloud parameterisations with data

We have simulated a climatological January and July. For each, we have performed 30 ensemble runs. This means that we have simulated each month 30 times, changing slightly the initial conditions. These 30 simulations are averaged for the present-day climate comparisons with satellite data.

In addition to the simulation using the original LMDZ parameterizations, we have performed one-month present-day simulations with the changes in the parameterizations discussed in Sect. 2. After several trials, we present a comparison of the parameterization configurations shown in Table 1.

Table 1: Summary of the LMDZ parameterization configurations tested in this study.

Model name	SSPs	v_m	ξ_{UT}
EC ξ_{UT} 0.4 (original LMDZ)	hexagonal columns	f(IWC)	0.4
Baran ξ_{UT} 0.4	complex particles	f(IWC)	0.4
Baran ξ_{UT} 0.3	complex particles	f(IWC)	0.3
Baran ξ_{UT} 0.25exp	complex particles	f(IWC)	$0.373\exp(-0.005p) + 0.128$, for $p < 400$ hPa
Baran ξ_{UT} $0.3x^2v_m$	complex particles	f(IWC,T)	$0.3 + (0.0014(p - 300))^2$, for $p < 300$ hPa

3.1 High cloud cover

High cloud cover in the GCM simulations is computed as grid cell coverage by cloud layers with a cloud top pressure < 440 hPa, assuming a maximum overlap between adjacent cloud layers and random overlap between cloud layers separated by layer(s) of clear sky.

For the evaluation of the simulated present-day climate high cloud cover, we use monthly averages of high cloud amount (CAH) from the updated GEWEX cloud assessment database (Stubenrauch et al. 2024; CAH files available at https://gewexca.aeris-data.fr/). This cloud amount corresponds to the one observed from satellites, with a view from above, for clouds with cloud top pressure < 440 hPa. Since lidar and IR sounders are the most sensitive to cirrus clouds, we use the datasets CALIPSO-ST (Science Team; Liu et al., 2019), CALIPSO-GOCCP (GCM-Oriented CALIPSO Cloud Products; Chepfer et al., 2010) and AIRS-CIRS (Clouds from IR Sounders; Stubenrauch et al., 2017).

CALIPSO-GOCCP and CALIPSO-ST essentially differ in the method of noise reduction: the first one uses vertical averaging while the second one uses horizontal averaging. CALIPSO-ST also uses an improved aerosol-cloud discrimination. In addition to the high cloud amount of the uppermost cloud layer (TOP_LAYER_CALIPSO-ST), CALIPSO-ST also reports CAH of high clouds with visible optical depth larger than 0.3 (PASSIVE_CALIPSO-ST).

https://doi.org/10.5194/egusphere-2026-5049
Preprint. Discussion started: 11 September 2026

While the lidar observes the real cloud top, the IR sounders determine a cloud height after having penetrated into it over an optical depth of about 0.5, slightly less and slightly more for opaque and semi-transparent clouds, respectively (Stubenrauch et al., 2017; Fig. 4a). This effect does not influence CAH of AIRS-CIRS in the tropics and subtropics, because the tropopause is high, but at higher latitudes where the tropopause decreases, some of the high clouds are moved into the category of mid-level clouds (Stubenrauch et al., 2024). Therefore, we only show the results of AIRS-CIRS between 30°N and 30°S.

Figure 3 presents the high cloud cover derived from these retrievals compared with the different present-day climate simulations, separately for a climatological January (a) and July (b).

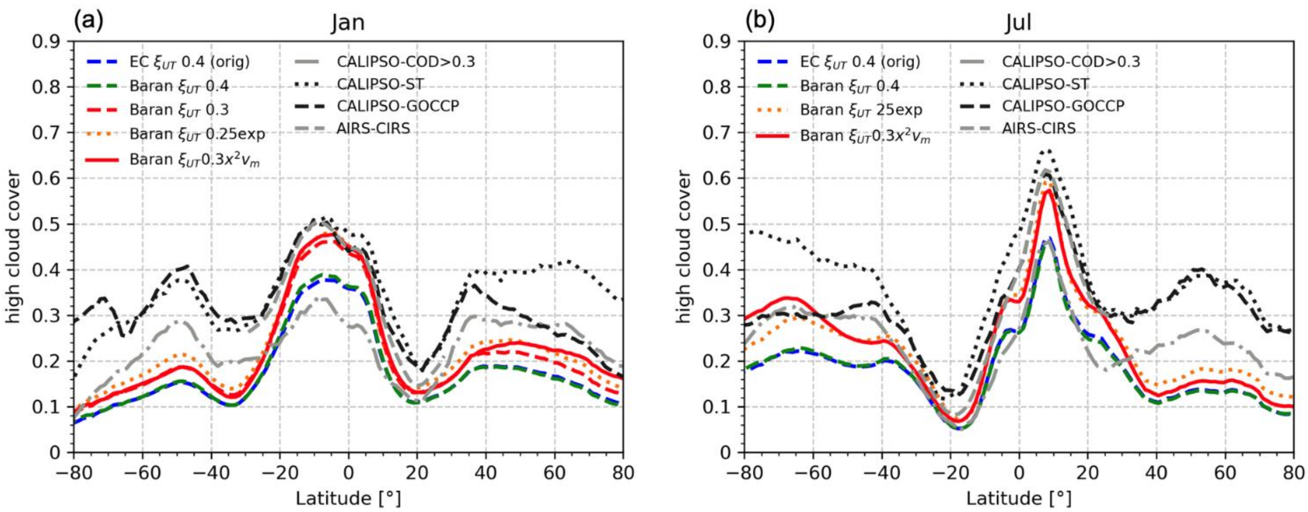

Figure 3: Zonal mean high cloud cover for a) January and b) July, from satellite retrievals (CALIPSO and AIRS) and from LMDZ present-day climate simulations using different parameters in the parameterizations concerning UT clouds.

The satellite retrievals show very similar results, except at latitudes higher than 40° during winter. The much larger CAH of CALIPSO-ST is linked to the detection of optically very thin clouds due to the better vertical resolution than of CALIPSO-GOCCP. It is interesting to note that UT clouds with an optical depth > 0.3 occur about 10% less. This explains the difference in high cloud cover at mid- and high latitudes during winter between CALIPSO-ST and CALIPSO-GOCCP.

The CAH of the original LMDZ simulation shows a latitudinal variation close to the one of the observations, in particular with the peak in the tropics, but CAH lies 0.1 to 0.2 below the observed values, both in January and in July. As expected, CAH is not sensitive to the change in the bulk microphysical ice cloud properties, but it is sensitive to ξ_{UT}, in particular in the tropics. By decreasing ξ_{UT} from 0.4 to 0.3, CAH increases in the tropics by about 0.1 and agrees very well with the observations. The change in the shape of $\xi_{UT}(p)$ is less relevant for CAH.

3.2 IWP

https://doi.org/10.5194/egusphere-2026-5049
Preprint. Discussion started: 11 September 2026

As we want to study the dynamical effect induced by the interaction between radiation and semi-transparent cirrus clouds (in-cloud IWP < 100 gm^{-2}), we need to verify the simulated IWP distributions. Since the IWP covers several orders of magnitude, distributions are difficult to compare (e. g. Eriksson et al., 2025). Therefore, we directly compare in Fig. 4 the fraction of tropical cases with the in-cloud IWP smaller than a certain threshold, as a function of this threshold.

Since satellite retrievals of in-cloud IWP use different vertical resolutions and assumptions on ice cloud microphysics, we compare the LMDZ present-day simulations to two datasets derived from combined lidar-radar measurements of the CALIPSO and CloudSat missions: DARDAR (raDAR-liDAR; Cazenave et al., 2019) and 2C-ICE (Deng et al., 2015). As the horizontal resolution of the radar footprint is about 2.5 km x 1.4 km, given on nadir tracks, we average the in-cloud IWP over 250 km. From Fig. 4 we deduce that the two retrievals give similar results, with 2C-ICE slightly more sensitive to thin cirrus: In the tropics, 45 to 55% of the detected UT ice clouds have an IWP < 10 gm^{-2}. About 85 to 90% of all tropical UT ice clouds have an IWP < 100 gm^{-2} (corresponding to a TOA warming effect according to Sokol et al., 2024).

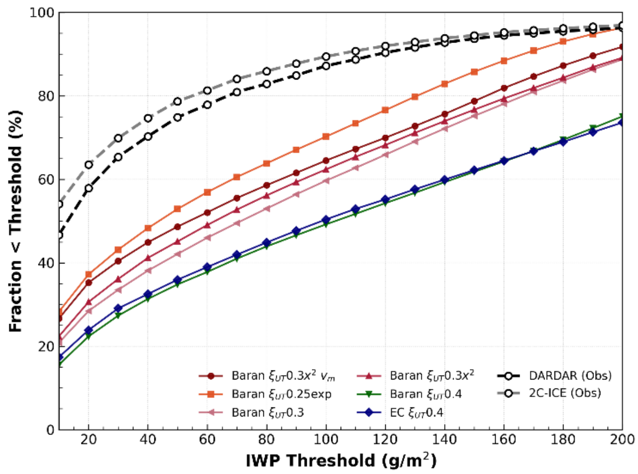

Figure 4: Fraction of cases with in-cloud IWP smaller than a certain threshold as function of this threshold, in the tropics (30°N-30°S), for two different satellite retrievals using CloudSat-CALIPSO data and for the LMDZ present-day climate simulations using different parameters in the parameterizations concerning UT clouds. Statistics of January.

When considering the LMDZ simulations, only 15 to 30% of the tropical UT ice clouds have an IWP < 10 gm^{-2}, and 47 to 70% have an IWP < 100 gm^{-2}. In particular, the original LMDZ parameterization leads to a tropical in-cloud IWP distribution which is far from the retrieved ones, with 47% instead of expected 85 to 90% of UT ice clouds with IWP < 100 gm^{-2}. Figure 4 also shows that the decrease in ξ_{UT} is the most efficient method to improve the fraction of UT clouds with IWP < 100 gm^{-2}. However, the IWP distribution is still shifted towards larger IWP values compared to the satellite retrievals. Changing from a constant to a p-dependent function like a square function increases more the thinner part of cirrus, and the change in the fall speed parameterization leads to a further improvement.

3.3 Diabatic heating

https://doi.org/10.5194/egusphere-2026-5049
Preprint. Discussion started: 11 September 2026

Since the CALIPSO-CloudSat data are only sampled along very narrow nadir tracks, Stubenrauch et al. (2021) have developed scene-dependent models, based on artificial neural network regression and trained with NASA CloudSat-lidar FLXHR radiative heating rates (v4; Henderson et al., 2013), to be applied on AIRS-CIRS data in order to expand these heating rates in space (onto the AIRS orbits) and in time (2004-2018). We use these radiative heating fields of the CIRS-ML dataset (available at https://gewex-utcc-proes.aeris-data.fr/data/), given at a spatial resolution of 0.5° latitude x 0.5° longitude, for the comparison with the present-day climate simulations.

Before comparing these heating rates to those simulated, we need to bring them to a similar horizontal and vertical resolution. As the CIRS-ML radiative heating rates are given on 20 layers between 1000 and 100 hPa, we need to average the simulated heating rates, which are given at 45 layers. This affects mostly the layers in the lower troposphere, because from a height of 500 hPa upwards the vertical resolution of the simulations and of CIRS-ML is similar. Furthermore, we investigate the atmospheric cloud radiative effect over grid cells which are covered by more than 80% of high-level clouds. The atmospheric cloud radiative effect (ACRE) when these clouds are present, is then computed by subtracting the monthly mean clear sky radiative heating rates from the radiative heating rates averaged over 1.5° latitude x 2.5° longitude grid cells with a high cloud cover > 80%. These cases correspond to about 31% of all grid cells between 10°N and 20°S in January.

Figure 5 presents these ACRE profiles, separately for SW and LW, as well as the latent heating profiles, from CIRS-ML and from the simulations using the parameterizations described above. According to Voigt et al. (2024), the NASA FLXHR radiative heating rates may have a low bias of about 20% in the upper troposphere (above a height corresponding to 450 hPa). This is indicated by a 0.15-K/day-wide-grey-shading in the LW in Fig. 5.

As expected (e.g. Sepulveda Araya et al., 2025), ice crystal complexity leads to weaker ice cloud radiative heating: When comparing to the CIRS-ML observations, the SW ACRE profiles in Fig. 5a show a clear improvement in the UT heating when moving from single-scattering properties of hexagonal columns (Ebert and Curry, 1992) to the ones of more complex ice crystals (Baran et al., 2016). The other parameterizations do not affect anymore the SW ACRE.

The single-scattering properties also affect the LW ACRE profiles, with a decrease in the heating between 250 and 600 hPa when using more complex ice crystals in the radiative transfer, and again in better agreement with the observations as shown in Fig. 5b.

In general, the shape of the LW ACRE is similar to the one of CIRS-ML, with a cooling around 200 hPa, from contributions above high convective towers and thick anvils, and a warming below. While CIRS-ML show two other local minima of warming around 400 and 550 hPa, the simulations show only one further local minimum around 600 hPa. The observed secondary minima in the LW radiative heating profile likely reflect preferred cloud-layer boundaries associated with the multi-layer structure of tropical cloud systems. The single minimum in the simulations suggests that the model does not fully capture the observed vertical organization of tropical cloud layers, despite reproducing the dominant upper-tropospheric cooling above and heating within the UT clouds.

While the simulations show also another warming of the atmosphere above 150 hPa, the observations show indeed an increase in LW ACRE, but it stays below 0. This heating should be due to thin cirrus, which are optically thicker in the simulations

https://doi.org/10.5194/egusphere-2026-5049
Preprint. Discussion started: 11 September 2026

than in the observations, as derived from Fig. 4. Additionally, we expect the CIRS-ML LW ACRE to be slightly underestimated in the UT because of the difficulty of IR sounders to detect very thin cirrus in the tropical tropopause layer (TTL).

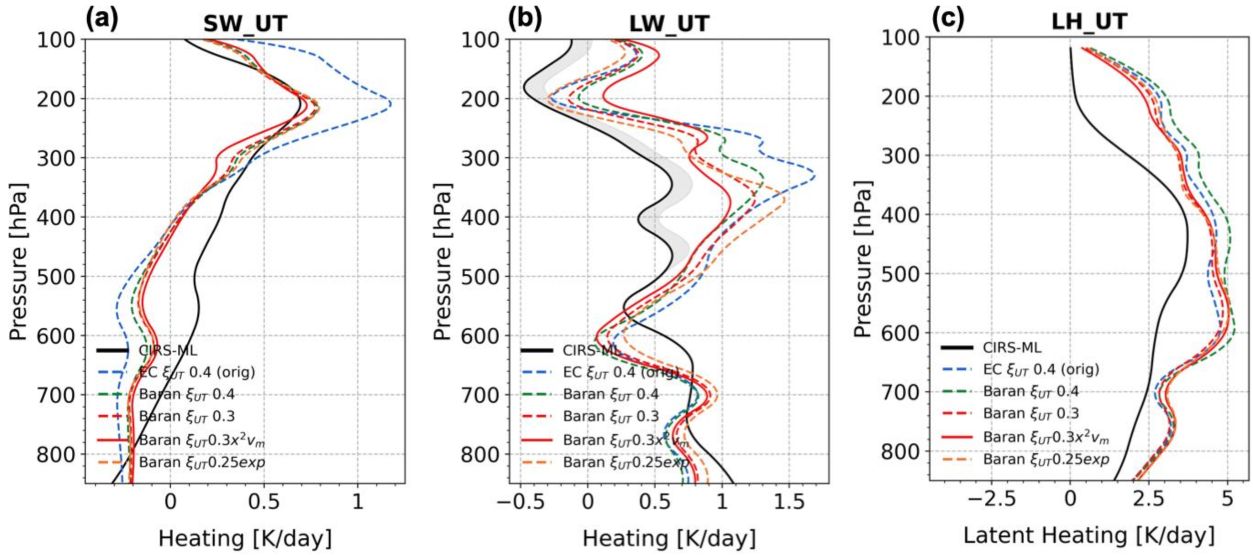

Figure 5: Profiles of atmospheric cloud radiative effect (ACRE), (a) SW and (b) LW, and of (c) latent heating, averaged over grid cells of 1.25° latitude x 2.5° longitude with more than 80% high-level cloud cover within the latitude band 10°N to 20°S in January. The simulations using the different parameterizations described above are compared to observations (CIRS-ML). The 0.15-K/day-wide-grey-shading indicates a plausible low-bias correction of the data in the UT.

Decreasing ξ_{UT} from 0.4 to 0.3 leads to a smaller heating between 250 and 350 hPa and a larger heating below. When changing to an exponentially increasing ξ_{UT} with height, this increases the vertical gradient of the heating rates, in slightly less agreement with the observations. Introducing a fall speed which also depends on T decreases the heating between 250 and 600 hPa further, in particular around 350 hPa, closer to the observations, while the cooling around 200 hPa decreased so much that on average it shows a slight warming. This can be explained by the fact that the ice crystals within the higher, thinner clouds do not fall as fast as the ones within the warmer thicker clouds.

Apart from the change in SSPs and a slight decrease in ξ_{UT}, which provide a clear improvement, the sensitivity to the change to a vertically dependent ξ_{UT} and to a T- and IWC- dependent fall speed, is of the same order (about 0.15 K/day) as the difference with the observations. Nevertheless, the simulations seem still to slightly overestimate the LW heating effect.

The latent heating of UT clouds depends less on these parameterizations, and the model produces slightly too much latent heating, as shown in Fig. 5c. Nevertheless, we observe that changing the SSPs alone has an increasing effect on the latent heating, while increasing the high cloud cover (and therefore making the clouds optically slightly thinner) has the opposite effect.

https://doi.org/10.5194/egusphere-2026-5049
Preprint. Discussion started: 11 September 2026

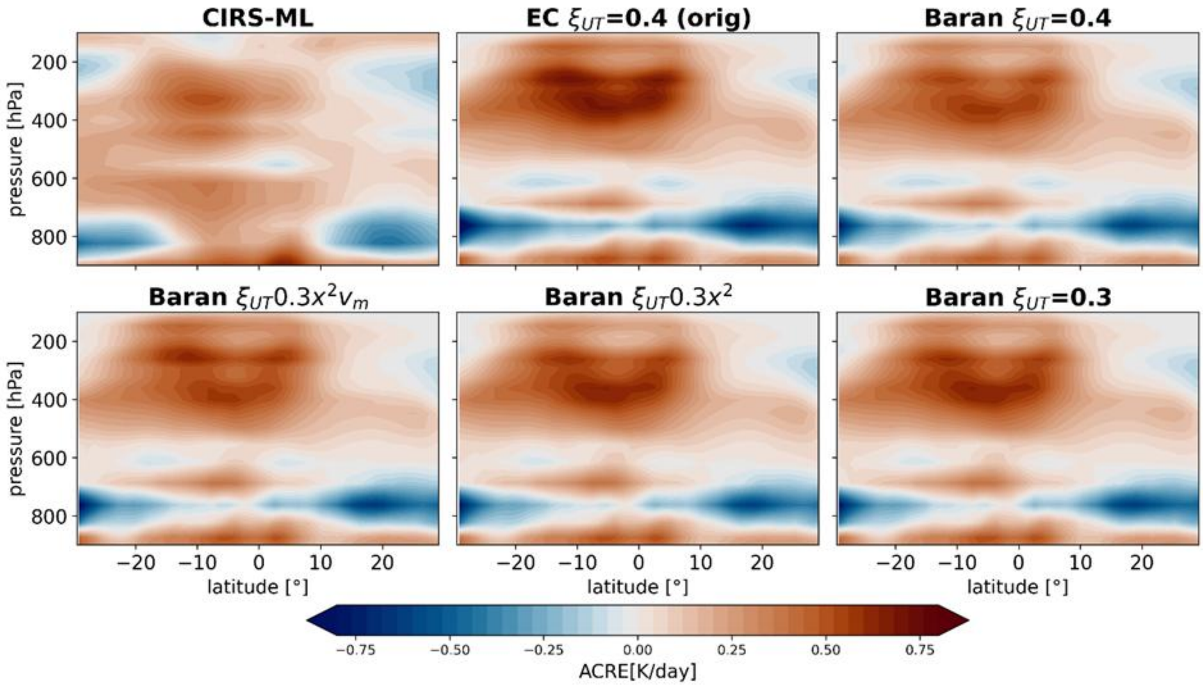

Figure 6: Zonally averaged profiles of atmospheric cloud radiative effect (ACRE), in January. The simulations using the different parameterizations described above are compared to the satellite retrievals (CIRS-ML, 2003-2018).

Figure 6 compares the zonal averages of the ACRE profiles for January between the satellite retrievals (CIRS-ML) and the simulations, again using the parameterizations described above. The conclusion is similar to that using the tropically averaged ACRE profiles of UT clouds. The original LMDZ code provides a heating between 200 and 500 hPa which is much larger than the one observed, and we observe an improvement when changing the parameterization of SSPs of ice crystals and when increasing the part of thinner UT ice clouds, by slightly decreasing the threshold of UT relative water variability as well as including a T-dependence in the fall speed.

Finally, we compare the relationship between the vertically integrated ACRE and the vertically integrated latent heating (LP). Figure 7 presents geographical maps of ACRE (colours) and LP (contours), for January and for July. Both the observations (CIRS-ML, top) and the simulations (original LMDZ with EC ξ_{UT}=0.4, middle, and Baran ξ_{UT}=0.3x^2 v_m parameterization, bottom) show a tight coupling between LP and ACRE: the ACRE is largest in regions of heavy precipitation (LP). The simulations agree relatively well with the observations, with slightly stronger LP gradients, as one would expect from the LH profiles in Fig. 5c. We also observe that the slightly smaller ACRE maxima when using the Baran ξ_{UT}=0.3x^2 v_m parameterization agree better with the data.

https://doi.org/10.5194/egusphere-2026-5049
Preprint. Discussion started: 11 September 2026

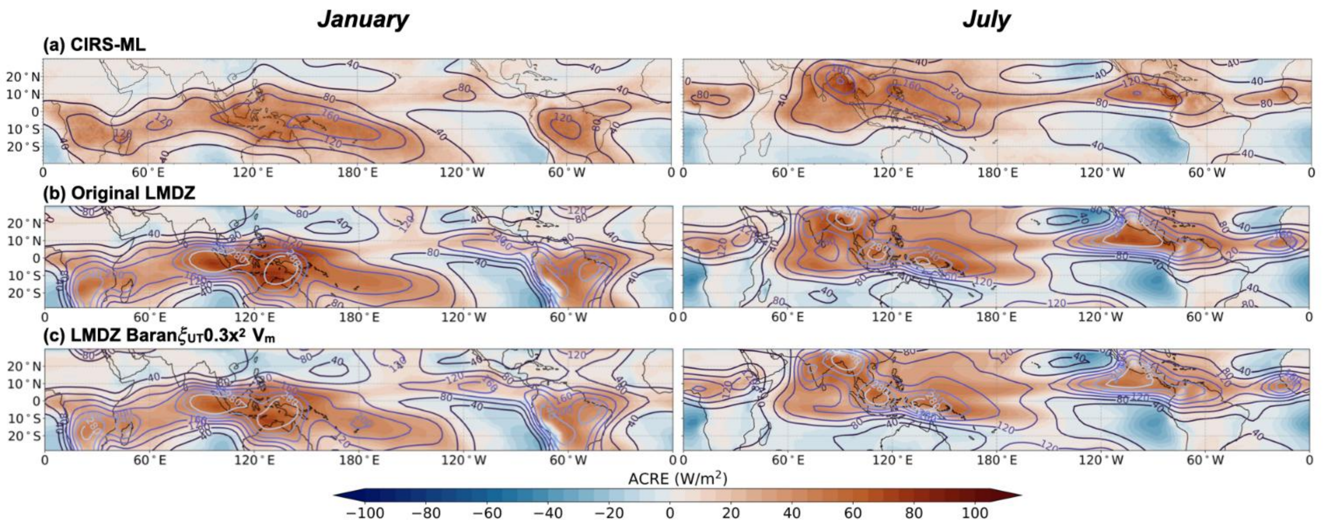

Figure 7: Geographical maps of vertically integrated atmospheric cloud radiative effect (ACRE, colours) and vertically integrated latent heating (LP, contours), in January (left) and in July (right), over the latitudes 30°N-30°S, at a spatial resolution of 2.5° x 2.5°. Panel rows (a) show observations from CIRS-ML (Chen et al., 2025). The present-day simulations are shown panel rows (b) and (c), using the initial LMDZ parameterizations and using Baran ξ_{UT}=0.3x^2 v$_m$, respectively.

4 Radiative impact of UT clouds on the Hadley circulation and on precipitation

The Hadley circulation transfers heat and moisture between the tropics and subtropics, playing an important role in setting precipitation and temperature patterns, and therefore has been studied extensively (e. g. Raymond, 2000; Chemke et al., 2019; Chen et al., 2020; De et al., 2021). Already, Rind and Rossow (1984) have highlighted that the Hadley circulation is sensitive to numerous processes and interactions that can produce small changes with large consequences and concluded that for a reliable prediction of changes in the Hadley circulation associated with climate warming one needs realistic representations of these processes.

Our study focuses on the radiative-dynamical interactions of UT clouds, differentiating between semi-transparent and opaque clouds.

In order to examine the radiative impact of the UT clouds on the dynamics, we have performed additional simulations in which we have made these clouds transparent to the radiation, (i) both to SW and LW radiation and (ii) to LW radiation alone, as it acts solely in the atmosphere. For each case, we have executed experiments with (1) only semi-transparent UT ice clouds and (2) all UT ice clouds transparent to radiation.

These simulations, together with the control runs (CTRL), allow us then to differentiate the radiative effects of semi-transparent UT clouds and the entire UT cloud population, by considering the differences CTRL - norad(IWP<100) and CTRL -

https://doi.org/10.5194/egusphere-2026-5049
Preprint. Discussion started: 11 September 2026

norad(hgh), respectively. In addition, the radiative effect of opaque clouds is determined from the difference norad(IWP<100) - norad(hgh), corresponding to CTRL – norad(opaq).

For climate simulations without UT cloud radiation interactions, we have modified the LMDZ module which prepares the cloud optical properties for the radiative transfer in the following way: First, UT ice cloud occurrence in a grid cell is identified by the maximum pressure layer with existing large-scale cloud ice ($q_{ice}^{in,lsc}(p) > 0$ gm^{-3}) being smaller than 400 hPa. For these grid cells, we compute the in-cloud IWP as the vertical integral of $q_{ice}^{in,lsc}$. For the SW and LW radiative transfer, we then reset in each layer with $q_{ice}^{in,lsc}(p) > 0$ gm^{-3} the cloud optical depth $\tau_{ice}(p) = 0$ for all grid cells with (1) 0 gm^{-2} < IWP < 100 gm^{-2} (norad(IWP<100) experiments) or (2) 0 gm^{-2} < IWP (norad(hgh) experiments). This approach considers the radiative impact of the ice part of large-scale UT clouds. According to a relatively smooth temperature dependence in the LMDZ (Madeleine et al., 2020), chosen to agree with CALIPSO observations (Choi et al. 2014; Cesana et al., 2015), the ice fraction corresponds to 100% of the condensed water for T(p) < -30°C, to 50% at T(p) = -25°C, to 20% at T(p) = -10°C and to 0% for T(p) > 0°C. This avoids in our no-radiation-interaction experiments large artificial heating at a fixed T, as shown by Haslehner et al. (2024) for studies using a fixed T threshold in a model which only permits ice to exist for T < -35°C (Gasparini et al., 2020).

Simulations have been performed for present-day climate, separately for January and July, using a) the original LMDZ (EC ξ_{UT}=0.4), b) SSPs of complex ice crystals in the radiative transfer (Baran ξ_{UT}=0.4), c) Baran ξ_{UT}=0.25exp and d) Baran $\xi_{UT}=0.3x^2\,v_m$. The latter two parameterizations lead to similar high cloud cover, but with a different vertical heating structure due to a differing v_m parameterization. Each time, we analyse results of 30 ensemble runs, after having tested that these are sufficient for our studies (by comparing with results from 100 ensemble runs).

Figure 8 presents the results for the combined SW and LW effect of UT clouds on the Hadley circulation, comparing averages over days 6 to 10 and over days 26 to 30 (adjusted equilibrium) in January, separately for the original LMDZ code and three variations of the UT cloud parameterizations discussed above. Results for July are displayed in Appendix B (Fig. B1) and for the LW effect alone in the supplement (Fig. S1 for January and Fig. S3 for July). From the high cloud cover in Fig. 3 we deduce that the Intertropical Convergence Zone (ITCZ) is approximately located between 20°S and 10°N (10°S and 20°N) in January (July).

Row (a) of Fig. 8 presents the zonally averaged stream function vertical sections of the control runs. The Hadley cell branch which connects the summer with the winter hemisphere is always the strongest, which is in January the Northern Hadley cell. In January, its clock-wise circulation starts the ascent at the core of the ITCZ (situated at about 8°S). Then the risen air flows across the equator into the Northern Hemisphere (UT divergence region), descends near 20°N (subsidence region) and finally flows back equatorward near the surface. The atmosphere transports energy via this cross-equatorial Hadley cell from the summer to the winter hemisphere. As the absolute values of the zonally averaged stream function profile are quite large, the behaviour looks similar for the different UT cloud parameterizations, though slightly stronger in the UT for the two last ones.

How is the Hadley circulation affected by the radiative interaction of semi-transparent UT clouds, of opaque UT clouds and of all UT clouds together, and how does this effect evolve over the system's adjustment? Therefore, we examine in Fig. 8 the

https://doi.org/10.5194/egusphere-2026-5049
Preprint. Discussion started: 11 September 2026

stream function profile differences CTRL - norad(IWP100), CTRL – norad(opaq) and CTRL -norad(hgh), at the beginning (rows b to d) and at the end (rows e to g) of the month of January.

The radiative effect of semi-transparent UT clouds on the Northern Hadley cell shows a weakening in the upper troposphere of the ascending branch of the cell immediately after the introduction of the perturbation (row b), similar for all four configurations. During the month, while the adjustment progresses, the Northern Hadley cell weakens further downwards and over the whole cell (row e) for the two parameterizations which have induced more, thinner UT clouds (columns 3 and 4). The introduction of a fall speed which depends on both IWC and T leads to the largest weakening through the whole atmospheric column, because by using this parameterization the thin UT clouds stay longer in the atmosphere than those sedimenting according to the original parameterization (Fig. 2).

On the other hand, the radiative interaction of opaque UT ice clouds strengthens the Northern Hadley cell, as deduced from rows (c and f) of Fig. 8. Again, this effect grows while the adjustment progresses, and it is stronger for the two parameterizations which lead to more UT clouds (columns 3 and 4). The strengthening is largest in the ascending and divergence branches. The weaker Southern Hadley cell is also slightly strengthened by this radiative effect.

The July simulations, presented in Fig. B1, show a similar radiative impact of the UT clouds on the Hadley circulation (this time the Southern cell, the cross-equatorial cell), with a weakening effect by the semi-transparent and a strengthening effect by the opaque UT clouds.

This means that, independent of the season, the radiative interaction of different UT cloud populations leads to opposite dynamical effects. Climate warming leads to a weaker Hadley circulation (e. g. Held and Soden, 2006; Kjellsson, 2015), in particular the cross-equatorial cell (e. g. Kang et al., 2013; Vallis et al., 2015). According to our findings, additional climate-warming-induced changes in the UT cloud optical depth will then enhance or weaken this behaviour.

The LW effect alone drives a large part of the dynamical impact (Fig. S1, rows b to g and Table S1). For semi-transparent UT clouds, the SW contribution is negligible, while for opaque UT clouds SW heating offsets part of the LW cooling above the cloud, reducing the vertical gradient there. Vertically integrated over the tropics, the ACRE is dominated by LW for both cloud types and both parameterizations, as shown in Table S1. Furthermore, the radiative interaction according to Baran ξ_{UT} $0.3x^2v_m$ parameterization leads to a larger ACRE than the EC ξ_{UT} 0.4 parameterization.

When the radiative effect of the whole UT cloud population is considered (rows d and g of Figs. 8 and B1, Figs.S1 and S3), the strengthening effect of the Hadley circulation predominates. This result is not in agreement with Haslehner et al. (2024) who concluded that the radiative interaction of high-level clouds do not have a significant impact on the Hadley cell strength. They came to that conclusion by comparing the maxima of the absolute values of the mass stream function within the free troposphere of the tropics (NH and SH), averaged over 30 years.

https://doi.org/10.5194/egusphere-2026-5049
Preprint. Discussion started: 11 September 2026

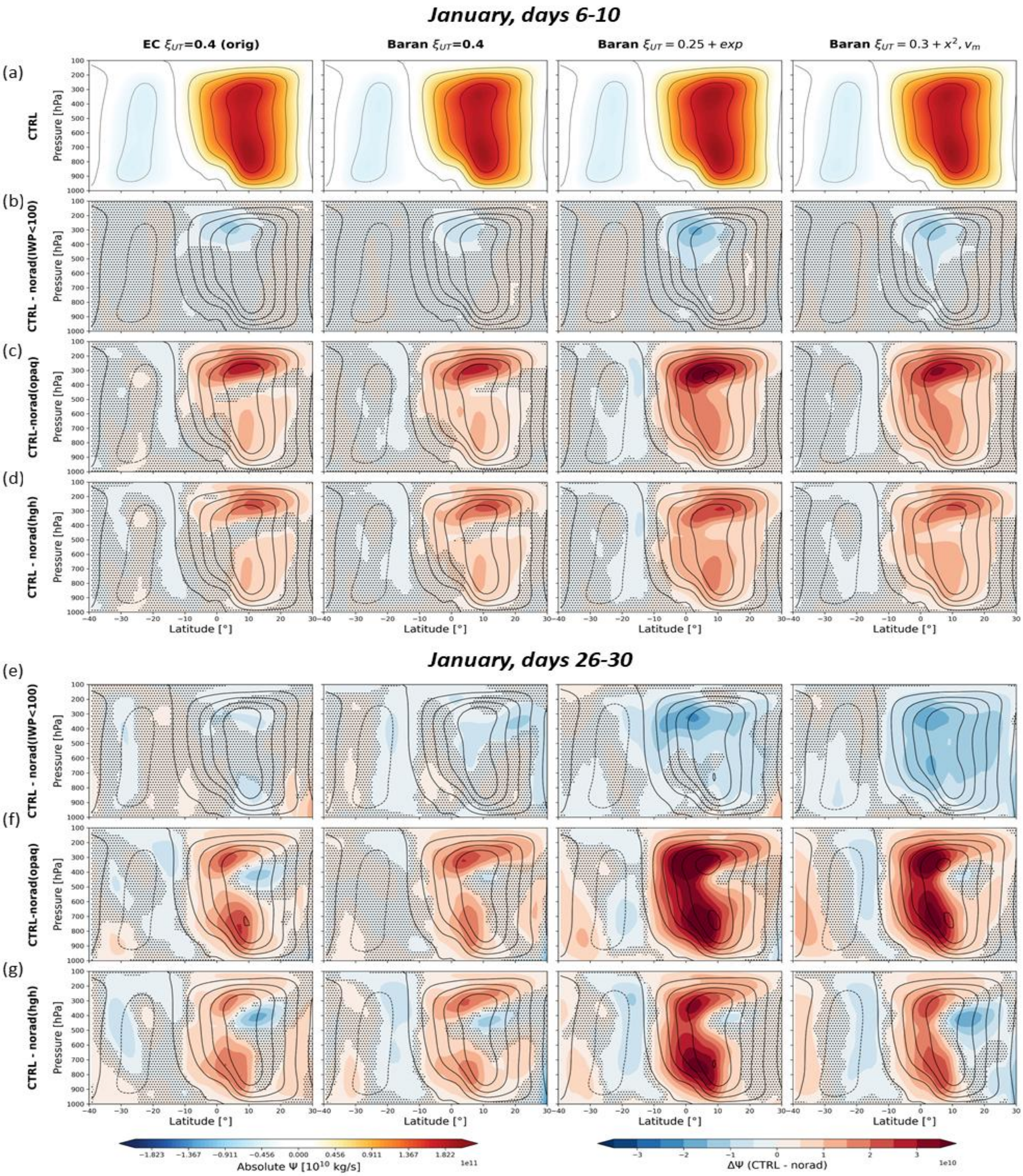

Figure 8: Zonally averaged stream function vertical sections (row a), and differences between CTRL and norad(IWP<100) (rows b and e), between CTRL and norad(opaq) (rows c and f) and between CTRL and norad(hgh) (rows d and g), for simulations using the four parameterizations described above (columns 1-4). Statistics considers days 6-10 (rows a-d) and days 26-30 (rows e-g) of present-day January transient simulations.

https://doi.org/10.5194/egusphere-2026-5049
Preprint. Discussion started: 11 September 2026

The vertical sections in Figs. 8g and B1g show clearly an overall strengthening. The relative radiative effect of opaque UT clouds on the maximum Hadley cell intensity within the tropical free troposphere is about 20% in January and 30% in July, using the parameterization Baran ξ_{UT}=0.3x^2 v_m, as shown in Table S1. The radiative, opposite effect of the semi-transparent UT clouds is smaller (about -11% in January and -6% in July), leaving the overall radiative effect of UT clouds positive and not negligible (9 to 25%). The seasonal difference in their effects may be due to maritime–continental ITCZ (see below). The effects using this parameterization are larger than the ones with the original one, which is especially seen by distinguishing semi-transparent and opaque clouds.

As we have shown that semi-transparent and opaque UT clouds have opposite effects, one reason for the disagreement may be that the UT clouds in the model simulations of Haslehner et al. (2024) are optically thinner, so that both effects cancel. Another reason for our disagreement with the conclusion of Haslehner et al. (2024) lies in the simulated heating profiles themselves: Fig. 5 of Haslehner et al. (2024) shows a high-level cloud atmospheric heating profile simulated by the ICON-ESM model which has its maximum much lower situated in the troposphere (5 to 7 km) than the retrieved heating rate profiles (10 to 12 km) and therefore may not be sufficient to strengthen the Hadley circulation significantly.

For a further investigation of the radiative-dynamical interactions of optically thin and optically thick UT clouds, we compare the zonal averages of the vertically integrated quantities ACRE, LP, as well as the mass-weighted vertically integrated moisture convergence (zonal mean vertical velocity multiplied by vertical derivative of zonal mean specific humidity) and dry static stability σ (vertical derivative of zonal mean potential temperature multiplied by the ratio of zonal mean temperature and potential temperature). Again, we distinguish radiatively active semi-transparent and opaque UT clouds. To separate the initial radiative effect and eventual feedbacks we consider the periods of days 6 to 10 and 26 to 30, respectively. Figure 9 presents absolute differences for the fluxes (ACRE, LP) and the moisture convergence and relative differences for the dry static stability, for January.

Though the ACRE, the initial forcing, is much smaller for the semi-transparent UT clouds than for the opaque UT clouds, their meridional behaviour is quite different: the semi-transparent UT clouds produce a heating at the edges of the ITCZ, in particular at the one in the winter hemisphere (so at the Northern one in January), whereas the opaque UT clouds produce a strong heating in the core of the ITCZ. The heating at the edges of the ITCZ, in regions of UT divergence, weakens this cooling and therefore the meridional heating gradient, while the strong heating in the core by the opaque UT clouds increases this gradient. So, the ACRE alone already explains the opposing Hadley circulation responses.

This heating only slightly changes throughout the simulation, but other quantities adjust, in particular when the radiative impact of opaque UT clouds is considered: We observe a decrease in LP (precipitation) at the edges of the ITCZ. A general tropical precipitation decrease has already been shown earlier and explained by the tropical energy balance (e. g. Li et al., 2015; Haslehner et al., 2024), in which it needs less LP to opposite the atmospheric radiative cooling which is reduced by the strong radiative heating of the UT clouds. According to Figs. 9 and B2, besides Table S1, our experiments also show a decrease in LP over the tropics, in January and in July.

https://doi.org/10.5194/egusphere-2026-5049
Preprint. Discussion started: 11 September 2026

The location of this LP decrease, which is in our simulations at the edges of ITCZ, can be explained by the intensification of the Hadley cell and therefore an intensified moisture convergence in the centre of the ITCZ which leaves the edges drying at the margins of the ITCZ. Both build up as the simulation advances in time.

Semi-transparent clouds do not alter the large-scale circulation strongly enough to organize moisture transport, leaving the precipitation fields to be governed locally. Nevertheless, Table S1 shows a systematic small tropical decrease of LP. The parameterizations lead to noise-like zonal mean LP differences which build up strongly progressively, reaching up to 10Wm^{-2}.

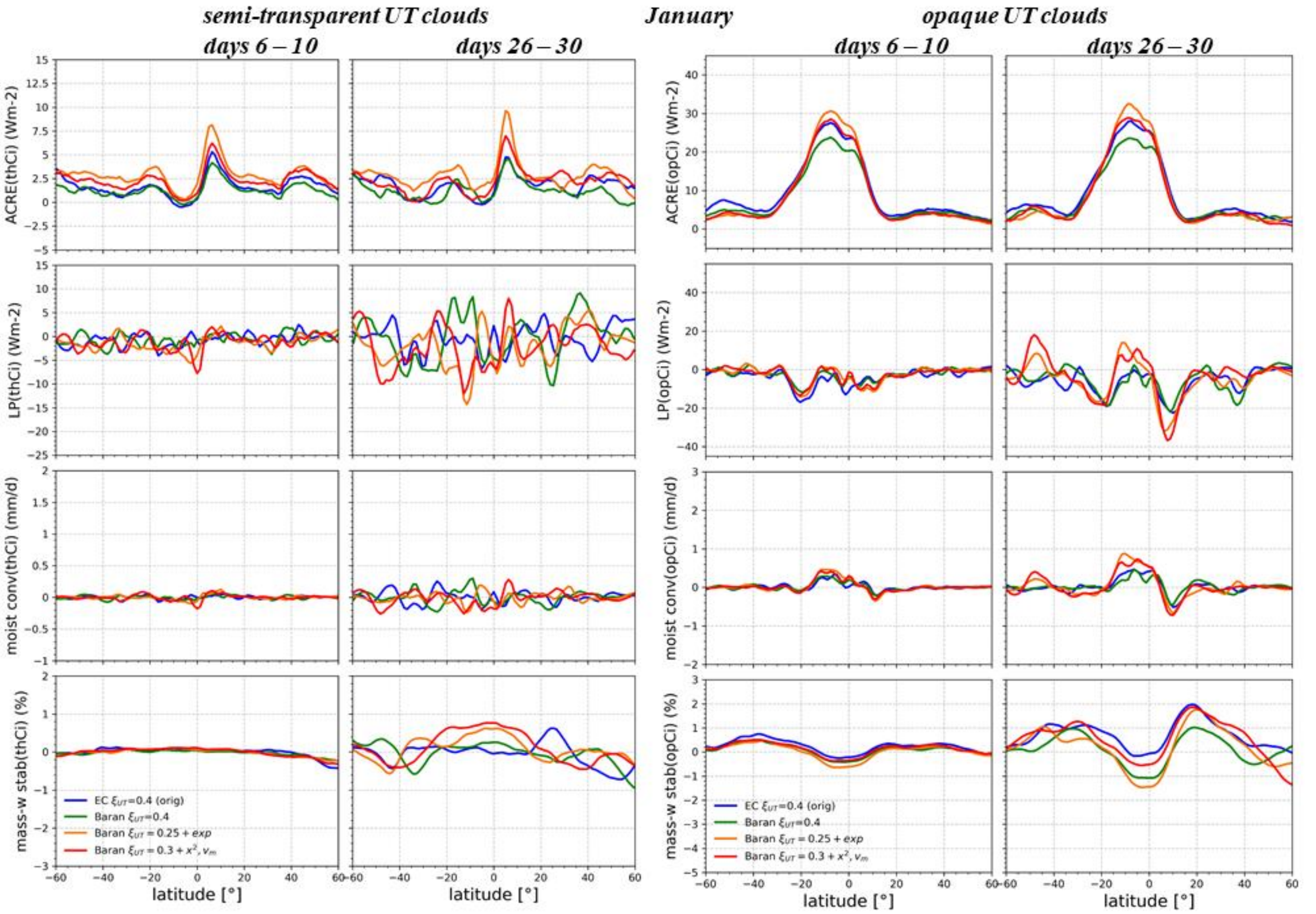

Figure 9: Zonal averages of ACRE, LP, mass-weighted vertically integrated moisture convergence and dry static stability, for CTRL – norad(IWP<100) and CTRL – norad(opaq) experiments, comparing different UT cloud parameterizations. The differences in the left panel show the radiative impact of semi-transparent UT clouds (columns 1-2), while those in the right panel show the one of opaque UT clouds (columns 3-4). Quantities averaged over days 6-10 (columns 1, 3) and days 26-30 (columns 2, 4) of present-day climate January.

The zonal mean stabilities also change over the course of the simulation. Though small, the adjustments in the stability differ between the two cloud types: The trapping of heat in the middle-to-lower troposphere and the LW cooling above the opaque UT clouds (e. g. Chen et al., 2025) steepen the local lapse rate, corresponding to a decrease of the potential temperature gradient

https://doi.org/10.5194/egusphere-2026-5049
Preprint. Discussion started: 11 September 2026

and therefore destabilize the core of the ITCZ. The stabilization outside is the atmospheric feedback trying to damp the accelerated circulation. The radiative impact of the semi-transparent UT clouds on the zonal mean stability is small and only apparent towards quasi-equilibrium for the two parameterizations with an increased UT cloud cover: Warming the upper troposphere decreases the lapse rate and leads to a weak uniform stabilizing over the tropical domain (20°S to 10°N).

While the difference with respect to the parameterizations is small in the beginning, it grows towards the quasi-equilibrium, revealing that the feedbacks linked to the initial radiative effect differ with these parameterizations. The two parameterizations which include more UT clouds (Baran ξ_{UT}=0.25exp and Baran ξ_{UT}=0.3x^2 v_m) lead to larger feedbacks.

The comparison between January and July allows us to study the variability due to the location of the ITCZ: The January ITCZ stands for deep convection mostly over ocean while the July ITCZ is dominated by deep convection over land.

In July (Figs. B2 and S3), the initial forcing (ACRE) of the semi-transparent UT clouds is again small and this time in the Southern hemisphere. However, ACRE of the opaque UT clouds has a huge peak around 10°N, over the land mass, corresponding to deep convective clouds with a strong vertical gradient (Chen et al., 2025). This destabilizes the atmosphere, causing a broad instability. This then gives rise to a narrow peak in the moisture convergence, pumping vast amounts of water vapour upward and causing a peak increase in LP. The small and broad decrease of LP at the Southern part of the ITCZ corresponds in this case to a small and broad decrease in moisture convergence, compared to the negative peak moisture convergence at the edge in January. In July, the maritime low-level monsoon winds transport water vapor northward rapidly toward the continental convective region, which has created a strong heat low. Despite the favourable, unstable environment, the precipitation is mainly governed by the moisture convergence and the strongest precipitation occurs where the continental-scale convergence and ascent occur.

5 Conclusions

The outcomes of this article are manifold. The first part of the article was devoted to presenting new observational metrics for the evaluation of UT cloud parameterizations in GCMs: (1) UT cloud radiative heating profiles and (2) fraction of ice clouds with IWP smaller than a certain threshold. Next, we assessed the radiative impact of semi-transparent and opaque UT clouds on the Hadley circulation and on precipitation. Furthermore, we demonstrated the sensitivity of the results due to UT cloud parameterizations.

The comparison of the tropical radiative heating rates of grid cells covered by UT clouds between CIRS-ML satellite observations and the LMDZ simulations clearly reveal that the parameterization of Baran et al. (2016), using single-scattering properties of complex ice crystals, is more realistic than the one of Ebert and Curry (1992) based on hexagonal columns. In particular, the reduced SW radiative heating is much more realistic. Furthermore, the reduction of the UT relative subgrid total water variablility ξ_{UT}, an essential parameter for the determination of UT cloud cover and IWP, brings the simulations even closer to the retrieved LW radiative heating rates. Changes in the p-dependence of ξ_{UT}, along with accounting for T in addition to IWP in the bulk ice fall speed parameterization, are smaller, but nonetheless alter the vertical shape of the LW heating rates.

https://doi.org/10.5194/egusphere-2026-5049
Preprint. Discussion started: 11 September 2026

To better assess the simulated amount of semi-transparent UT clouds (with an IWP < 100 gm^{-2}), we have compared the fraction of grid cells with UT clouds of an IWP smaller than a certain threshold as function of this IWP threshold between the simulations and CALIPSO-CloudSat satellite observations, the latter being averaged over a similar grid size. The original LMDZ simulations, with the configuration for CMIP6, show a fraction of about 47%, compared to about 85 to 90% expected from two independent retrievals. This fraction improved to around 65% with the parameterization changes described above. Moreover, it is important to assess several variables, as a parameterization which improves the simulated amount of semi-transparent UT clouds may deteriorate the vertical shape of the LW heating rate.

The second part of this article investigated radiative-dynamical interactions of UT clouds. Particularly, we differentiated the effects of tropical semi-transparent and opaque UT clouds on the Hadley circulation and their feedback on meridional precipitation patterns. For the numerical experiments, we made these types of clouds transparent to the radiation by setting their layer optical depths to 0 for the radiative transfer computations.

These experiments demonstrated that the radiative interaction of these two UT cloud type populations provoke opposite dynamical effects: Whereas the semi-transparent UT clouds at the edge of the ITCZ reduce the meridional heating gradient and therefore weaken the Hadley circulation, the opaque UT clouds with their large vertically integrated ACRE in the core of the ITCZ strengthen the circulation. These effects are similar in January and in July. This means that climate- warming driven changes in the optical depth distribution of tropical UT clouds may then additionally alter (enhance or counteract) the climate-warming-driven weakening of the Hadley circulation.

Semi-transparent UT clouds do not alter the large-scale circulation strongly enough to organize moisture transport and therefore only locally affect the precipitation patterns. Yet, the noise of the meridional variation of the vertically integrated LH due to the different UT cloud parameterization increases strongly towards the quasi-equilibrium, in particular if one only considers the LW interaction (acting on the atmosphere alone). This indicates that the feedbacks linked to the initial radiative effect differ strongly with these parameterizations.

As the strong positive cloud radiative effect of opaque UT clouds diminishes the requirement for condensational heating to counteract the atmosphere's net radiative cooling, an overall suppression of tropical precipitation is driven by thermodynamic constraints. However, the location of this decrease is governed by a dynamic adjustment via moisture convergence, as the precipitation drops rather at the edges of the ITCZ than uniformly. The extent of this precipitation decrease at these edges (peaks and width) depends on the mode of the ITCZ (oceanic or continental):

In January (oceanic ITCZ), the core-concentrated radiative heating accelerates the cross-equatorial Hadley overturning, dynamically importing moisture into the central updraft and leaving the ITCZ margins moisture-starved, which localizes the thermodynamic precipitation reduction at the edges.

In July, the land-based deep convective cloud heating, with strong vertical gradient, has a huge peak around 10°N. This destabilizes the atmosphere, leading to a broad instability. Despite the favourable, unstable environment, the precipitation is mainly governed by the moisture convergence, with a narrow peak around the continental-scale convergence and ascent, while the precipitation reduction shows a broader and less pronounced behaviour.

https://doi.org/10.5194/egusphere-2026-5049
Preprint. Discussion started: 11 September 2026

Though the radiative effect of semi-transparent UT clouds on the Hadley circulation is smaller than the one of opaque UT clouds, it is opposite in sign. Simulations using UT cloud parameterizations that better reproduce observations lead to more coherent results in our experiments on radiative-dynamical interactions. We have to keep in mind that the amount of thin cirrus is still underestimated in the LMDZ model. The observations and analysis tools provided here will help further improve these parameterizations.

These numerical experiments have been undertaken with a GCM of a relatively coarse spatial resolution, in which the large-scale UT clouds are formed at each time step and organisation of convection is not explicitly represented. It would be interesting to investigate these radiative effects on atmospheric dynamics with global cloud-resolving models.

Appendix A: Scattering correction for the computation of LW fluxes

For the computation of LW fluxes in the LMDZ code, we have corrected the cloud optical depth for scattering effects by first taking out the forward peak contribution (estimated as $f = g^2$) from k_{ext}, ω_0 and g, using the δ-function adjustment, and then using these scaled variables to recompute the diffusion / two-stream effective optical depth (Joseph et al. 1976):

$$k_{ext}' = k_{ext} * (1. - \omega_0 * g^2) \quad \text{(A1)}$$

$$\omega_0' = (1. - g^2) * \omega_0 / (1. - \omega_0 * g^2) \quad \text{(A2)}$$

$$g' = (g - g^2) / (1. - g^2) \quad \text{(A3)}$$

$$\tau' = k_{ext}' * \sqrt{(3 * (1.- \omega_0') * (1.- \omega_0' * g'))} * IWP \quad \text{(A4)}$$

with $\sqrt{(3 * (1.- \omega_0') * (1.- \omega_0' * g'))}$ replacing the diffusivity factor 1.66 in the original LMDZ formulation.

Appendix B: Radiative impact of UT clouds on the Hadley circulation and precipitation in July

The following figures are the same as Figures 8 and 9, but for July simulations.

https://doi.org/10.5194/egusphere-2026-5049
Preprint. Discussion started: 11 September 2026

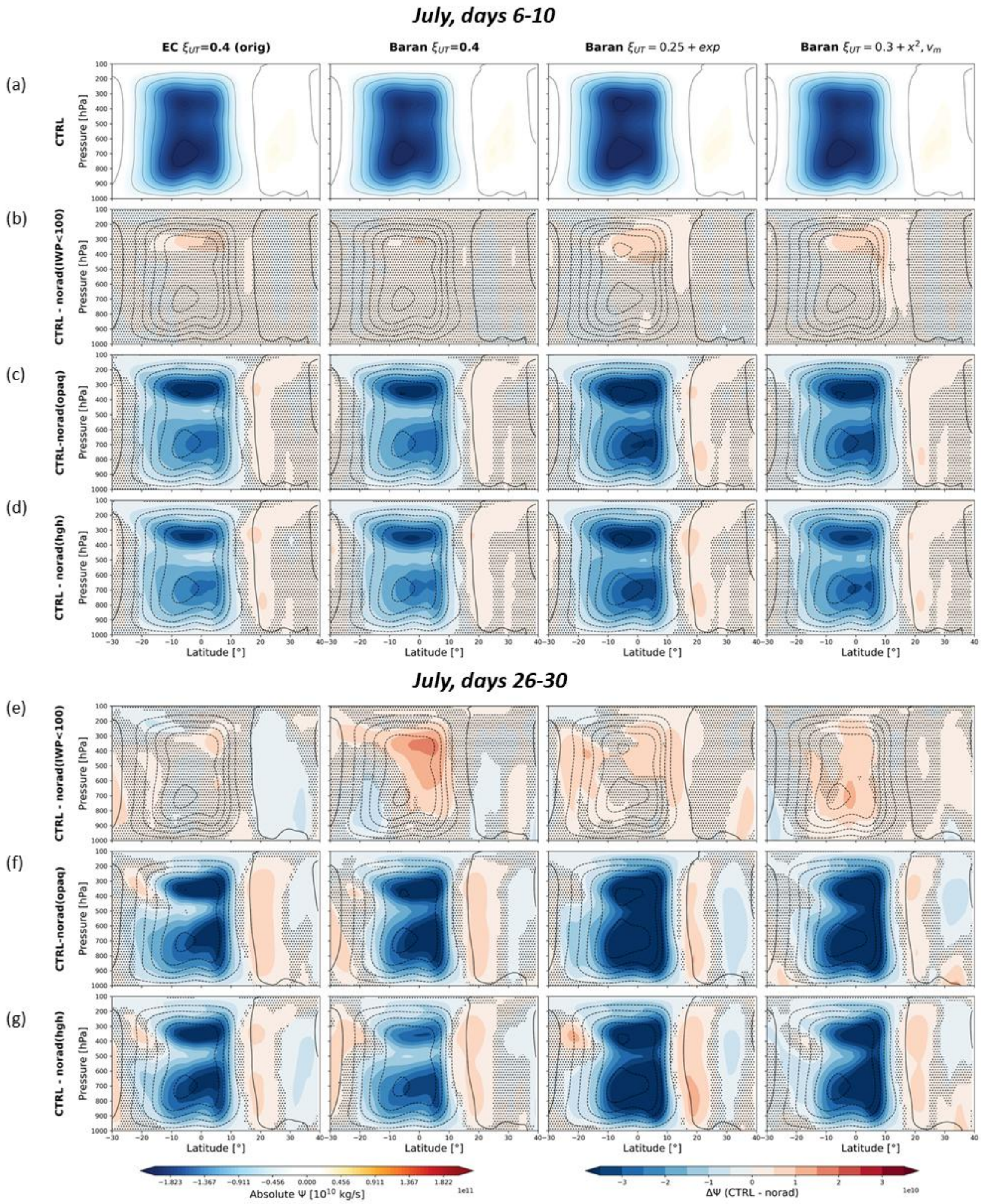

500 **Figure B1: Zonally averaged stream function vertical sections (row a), and differences between CTRL and norad(IWP<100) (rows b and e), between CTRL and norad(opaq) (rows c and f) and between CTRL and norad(hgh) (rows d and g), for simulations using the four parameterizations described above (columns 1-4). Statistics considers days 6-10 (rows a-d) and days 26-30 (rows e-g) of present-day July transient simulations.**

https://doi.org/10.5194/egusphere-2026-5049
Preprint. Discussion started: 11 September 2026

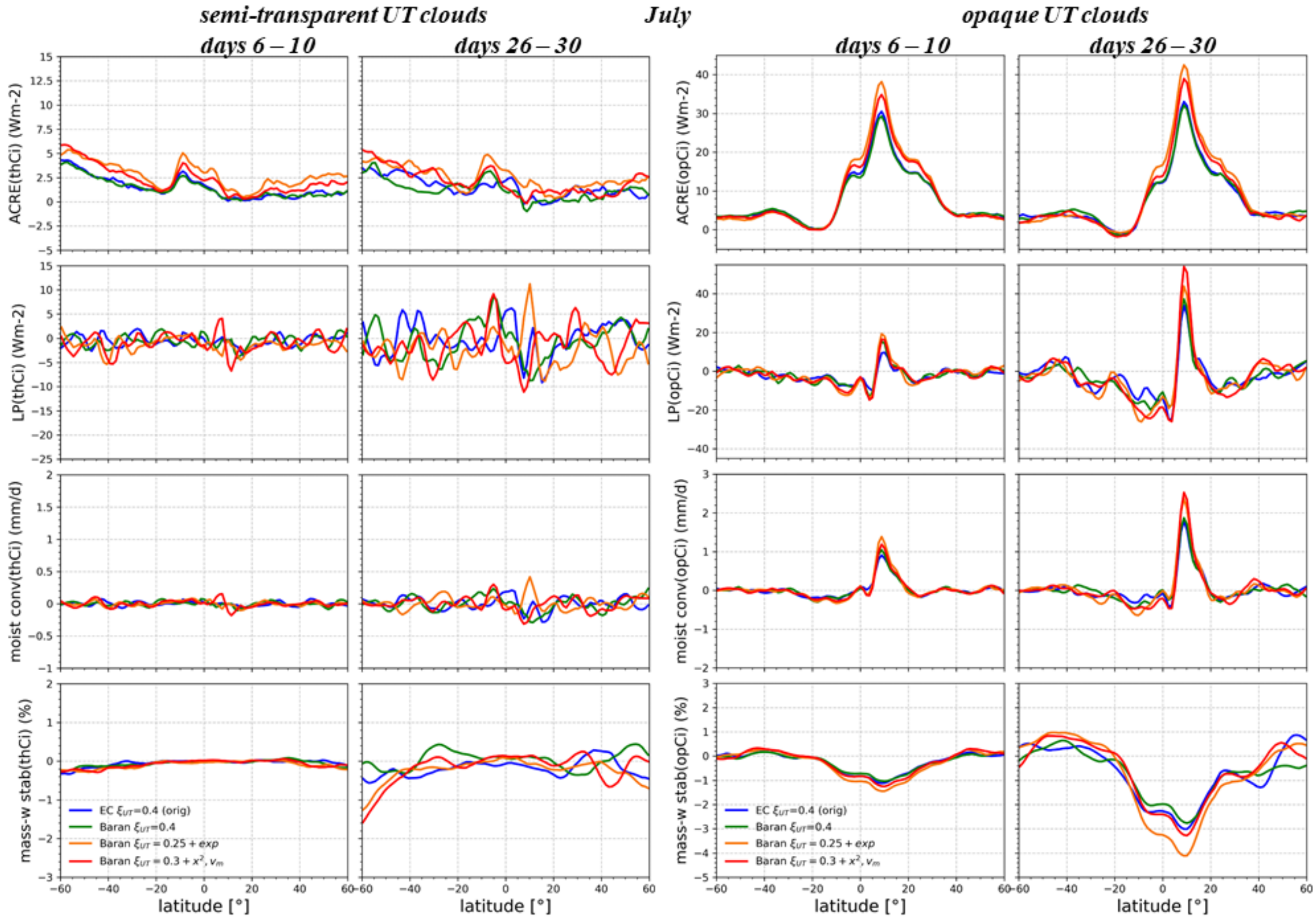

Figure B2: Zonal averages of ACRE, LP, mass-weighted vertically integrated moisture convergence and dry static stability, for CTRL – norad(IWP<100) and CTRL – norad(opaq) experiments, comparing different UT cloud parameterizations. The differences in the left panel show the radiative impact of semi-transparent UT clouds (columns 1-2), while those in the right panel show the one of opaque UT clouds (columns 3-4). Quantities averaged over days 6-10 (columns 1, 3) and days 26-30 (columns 2, 4) of present-day climate July.

Code and data availability

The CIRS-ML radiative heating rates are distributed by the French Data Center AERIS (Data and Services for the Atmosphere) via the website for the Process Evaluation Study of Upper tropospheric Clouds and Convection of the Global Energy and Water Exchanges Program (GEWEX UTCC PROES) at https://gewex-utcc-proes.aeris-data.fr/ (CIRS-ML; Stubenrauch et al., 2021; last access: 25 June 2025). A code for the comparison of radiative heating rates between simulations and these observations will be made available also on this website. The updated GEWEX cloud assessment database is distributed by the French data centre AERIS at https://gewexca.aeris-data.fr/ (Stubenrauch et al., 2024; last access: 5 August 2026). A code

https://doi.org/10.5194/egusphere-2026-5049
Preprint. Discussion started: 11 September 2026

for a comparison of high-level cloud cover between simulations and these observations will also be made available on this website. The IWP data from NASA 2C-ICE (https://www.cloudsat.cira.colostate.edu/data-products/2c-ice) and DARDAR (https://www.icare.univ-lille.fr/dardar/) have been downloaded by the IPSL ESPRI Mesocenter.

Supplement link

The link to the supplement will be included by Copernicus.

Author contributions

XC and CJS analysed the data and simulations. CJS, XC and LL designed the simulation experiments. CJS changed the model code, XC and LL performed the simulations. AJB provided help for the implementation of the complex ice SSP parameterization into the model code. CJS prepared the manuscript with contributions from all co-authors, in particular XC.

Competing interests

The contact author has declared that none of the authors has any competing interests.

Disclaimer

Copernicus Publications remains neutral with regard to jurisdictional claims made in the text, published maps, institutional affiliations, or any other geographical representation in this paper. While Copernicus Publications makes every effort to include appropriate place names, the final responsibility lies with the authors. Views expressed in the text are those of the authors and do not necessarily reflect the views of the publisher.

Acknowledgements

We gratefully acknowledge the efforts and collaboration of the AIRS, CALIPSO and CloudSat science teams for providing the datasets used in this study. We also extend our thanks to the engineers and space agencies whose work ensures the consistent quality of these data. The computational resources provided by the IPSL ESPRI Mesocenter were instrumental to the completion of this work. Our special thanks go to Blaž Gasparini, Sylvia Sullivan and William B. Rossow for insightful discussions and to Ionela Musat for help with the LMDZ code. Finally, we would like to acknowledge the use of Fabio Crameri's scientific colour maps (Crameri et al., 2020) in the preparation of some of our figures, which adhere to the principles of readability and accessibility in scientific visualization.

https://doi.org/10.5194/egusphere-2026-5049
Preprint. Discussion started: 11 September 2026

Financial support

This work has been supported by the China Scholarship Council (CSC) programme (grant no. 202208070008), and the French National Centre for Scientific Research (CNRS).

Review statement

The review statement will be added by Copernicus Publications listing the handling editor as well as all contributing referees according to their status anonymous or identified.

References

Baran, A. J., Hill, P., Furtado, K., Field, P., and Manners, J.: A Coupled Cloud Physics–Radiation Parameterization of the Bulk Optical Properties of Cirrus and Its Impact on the Met Office Unified Model Global Atmosphere 5.0 Configuration, J. Climate, 27, 7725–7752, https://doi.org//10.1175/JCLI-D-13-00700.1, 2014.

Baran, A. J., Hill, P., Walters, D., Hardiman, S. C., Furtado, K., Field, P. R., and Manners, J.: The Impact of Two Coupled Cirrus Microphysics–Radiation Parameterizations on the Temperature and Specific Humidity Biases in the Tropical Tropopause Layer in a Climate Model, J. Climate, 29, 5299–5316, https://doi.org/10.1175/JCLI-D-15-0821.1, 2016.

Bergman, J. W., and Hendon, H. H.: Cloud Radiative Forcing of the Low-Latitude Tropospheric Circulation: Linear Calculations, J. Atmos. Sci., 57, 2225-2245, https://doi.org/10.1175/1520-0469(2000)057<2225:CRFOTL>2.0.CO;2, 2000.

Bony, S., Stevens, B., Coppin, D., Becker, T., Reed, K. A., Voigt, A., and Medeiros, B.: Thermodynamic control of anvil cloud amount, PNAS, 113, 8927-8932, https://doi.org/10.1073/pnas.1601472113, 2016.

Byrne, M. P. and Schneider, T.: Atmospheric Dynamics Feedback: Concept, Simulations, and Climate Implications, J. Climate, 31, 3249–3264, https://doi.org/10.1175/JCLI-D-17-0470.1, 2018.

Cazenave, Q., Ceccaldi, M., Delanoë, J., Pelon, J., Groß, S., and Heymsfield, A.: Evolution of DARDAR-CLOUD ice cloud retrievals: new parameters and impacts on the retrieved microphysical properties, Atmos. Meas. Tech., 12, 2819–2835, https://doi.org/10.5194/amt-12-2819-2019, 2019.

Cesana, G., Waliser, D. E., Jiang, X., and Li, J. L.: Multimodel evaluation of cloud phase transition using satellite and reanalysis data, J. Geophys. Res. Atmospheres, 120, 7871-7892, https://doi.org/10.1002/2014JD022932, 2015.

Chemke, R., and Polvani, L. M.: Opposite tropical circulation trends in climate models and in reanalyses, Nature Geoscience, 12, 528-532, https://doi.org/10.1038/s41561-019-0383-x, 2019.

Chen, X., Pauluis, O. M., Leung, L. R., and Zhang, F.: Significant contribution of mesoscale overturning to tropical mass and energy transport revealed by the ERA5 reanalysis, Geophys. Res. Lett., 47, e2019GL085333, https://doi.org/10.1029/2019GL085333, 2020.

https://doi.org/10.5194/egusphere-2026-5049
Preprint. Discussion started: 11 September 2026

Chen, X., Stubenrauch, C. J., and Mandorli, G.: Relationship between latent and radiative heating fields of tropical cloud systems using synergistic satellite observations, Atmos. Chem. Phys., 25, 6857–6880, https://doi.org/10.5194/acp-25-6857-2025, 2025.

Chepfer H., Bony, S., Winker, D., Cesana, G., Dufresne, J. L., Minnis, P., Stubenrauch, C. J., and Zeng, S.: The GCM-oriented CALIPSO Cloud Product (CALIPSO-GOCCP), J. Geophys. Res. Atmospheres, 115, https://doi.org/10.1029/2009JD012251, 2010.

Choi, Y. S., Ho, C. H., Park, C. E., Storelvmo, T., and Tan, I.: Influence of cloud phase composition on climate feedbacks, J. Geophys. Res. Atmospheres, 119, 3687-3700, https://doi.org/10.1002/2013JD020582, 2014.

De, B., Tselioudis, G., and Polvani, L. M.: Improved representation of atmospheric dynamics in CMIP6 models removes climate sensitivity dependence on Hadley cell climatological extent, Atmos. Sci. Lett., 23, e1073, https://doi.org/10.1002/asl.1073, 2022.

Del Genio, A. D., Kovari, W., Yao, M.-S., and Jonas, J.: Cumulus Microphysics and Climate Sensitivity, J. Climate, 18, 2376–2387, https://doi.org/10.1175/JCLI3413.1, 2005.

Deng, M. and Mace, G. G.: Cirrus Cloud Microphysical Properties and Air Motion Statistics Using Cloud Radar Doppler Moments: Water Content, Particle Size, and Sedimentation Relationships, Geophys. Res. Lett., 35, 2008GL035054, https://doi.org/10.1029/2008GL035054, 2008.

Deng, M., Mace, G., Wang, Z., and Berry, E.: CloudSat 2C-ICE product update with a new Ze parameterization in lidar-only region, J. Geophys. Res., 120, 12198–12208, https://doi.org/10.1002/2015JD023600, 2015.

Ebert, E. E., and Curry, J. A.: A Parameterization of Ice Cloud Optical Properties for Climate Models, J. Geophys. Res. Atmospheres, 97, 3831–3836, https://doi.org/10.1029/91JD02472, 1992.

Eriksson, P., Baró Pérez, A., Müller, N., Hallborn, H., May, E., Brath, M., Buehler, S. A., and Ickes, L.: Advancements and continued challenges in observations and global modelling of atmospheric ice mass, Atmos. Chem. Phys., 26, 2741–2768, https://doi.org/10.5194/acp-26-2741-2026, 2026.

Field, P. R., Heymsfield, A. J., and Bansemer, A.: Snow Size Distribution Parameterization for Midlatitude and Tropical Ice Clouds, J. Atmos. Sci., 64, 4346–4365, https://doi.org/10.1175/2007JAS2344.1, 2007.

Gasparini, B., McGraw, Z., Storelvmo, T., and Lohmann, U.: To what extent can cirrus cloud seeding counteract global warming?. Environ. Res. Lett., 15, 054002, https://doi.org/10.1088/1748-9326/ab71a3, 2020.

Gehlot, S. and Quaas, J.: Convection–Climate Feedbacks in the ECHAM5 General Circulation Model: Evaluation of Cirrus Cloud Life Cycles with ISCCP Satellite Data from a Lagrangian Trajectory Perspective, J. Climate, 25, 5241-5259, https://doi.org/10.1175/JCLI- D- 11-00345.1, 2012.

Haslehner, K., Gasparini, B., Voigt, A.: Radiative Heating of High-Level Clouds and its Impacts on Climate, J. Geophys. Res. Atmospheres, 129, e2024JD040850, https://doi.org/10.22541/essoar.170612250.06578970/v1, 2024.

Held, I., and Soden, B.: Robust Responses of the Hydrological Cycle to Global Warming, J. Climate, 19, 5686–5699, https://doi.org/10.1175/JCLI3990.1, 2006.

https://doi.org/10.5194/egusphere-2026-5049
Preprint. Discussion started: 11 September 2026

Henderson, D. S., L'Ecuyer, T., Stephens, G., Partain, P., and Sekiguchi, M.: A Multisensor Perspective on the Radiative Impacts of Clouds and Aerosols, J. Appl. Meteor. Climat., 52, 853-871, https://doi.org/10.1175/JAMC-D-12-025.1, 2013.

Heymsfield, A. J., and Donner, L. J.: A Scheme for Parameterizing Ice-Cloud Water Content in General Circulation Models, J. Atmos. Sci., 47, 1865–1877, https://doi.org/10.1175/1520-0469(1990)047<1865:ASFPIC>2.0.CO;2, 1990.

Joseph, J. H., Wiscombe, W. J., and Weinman, J. A.: The delta-Eddington approximation for radiative flux transfer, J. Atmos. Sci., 33, 2452–2459, https://doi.org/10.1175/1520-0469(1976)033<2452:TDEAFR>2.0.CO;2, 1976.

Iacobellis, S. F., and Somerville, R. C. J.: Implications of Microphysics for Cloud-Radiation Parameterizations: Lessons from TOGA COARE, J. Atmos. Sci., 57, 161–183, https://doi.org/10.1175/1520-0469(2000)057<0161:IOMFCR>2.0.CO;2, 2000.

Kang, S. M., Deser, C., and Polvani, L. M.: Uncertainty in climate change projections of the Hadley circulation: The role of internal variability, J. Climate, 26, 7541-7554, https://doi.org/10.1175/JCLI-D-12-00788.1, 2013.

Kjellsson, J.: Weakening of the global atmospheric circulation with global warming, Clim. Dyn., 45, 975-988, https://doi.org/10.1007/s00382-014-2337-8, 2015.

Li, Y., Thompson, D. W., and Bony, S.: The influence of atmospheric cloud radiative effects on the large-scale atmospheric circulation, J. Climate, 28, 7263-7278, https://doi.org/10.1175/JCLI-D-14-00825.1, 2015.

Liu, Z., Kar, J., Zeng, S., Tackett, J., Vaughan, M., Avery, M., Pelon, J., Getzewich, B., Lee, K.-P., Magill, B., Omar, A., Lucker, P., Trepte, C., and Winker, D.: Discriminating between Clouds and Aerosols in the CALIOP Version 4.1 Data Products, Atmos. Measure. Tech., 12, 703–734, https://doi.org/10.5194/amt-12-703-2019, 2019.

Lohmann, U., and Roeckner, E.: Influence of cirrus cloud radiative forcing on climate and climate sensitivity in a general circulation model, J. Geophys. Res., 100, 16305–16323, https://doi.org/10.1029/95JD01383, 1995.

Madeleine, J.-B., Hourdin, F., Grandpeix, J.-Y., Rio, C., Dufresne, J.-L., Vignon, E., et al.: Improved representation of clouds in the atmospheric component LMDZ6A of the IPSL-CM6A Earth system model, J. Advanc. Modeling Earth Systems, 12, e2020MS002046, https://doi.org/10.1029/2020MS002046, 2020.

Mauritsen, T., and Stevens, B.: Missing iris effect as a possible cause of muted hydrological change and high climate sensitivity in models, Nat. Geosci., 8, 346-351, https://doi.org/10.1038/ngeo2414, 2015.

Mitchell, D. L., Mishra, S., and Lawson, R. P.: Representing the Ice Fall Speed in Climate Models: Results from Tropical Composition, Cloud and Climate Coupling (TC4) and the Indirect and Semi-Direct Aerosol Campaign (ISDAC), J. Geophys. Res., 116, D00T03, https://doi.org/10.1029/2010JD015433, 2011.

Mlawer, E. J., Taubman, S. J., Brown, P. D., Iacono, M. J., and Clough, S. A.: Radiative transfer for inhomogeneous atmospheres: RRTM, a validated correlated-k model for the longwave, J. Geophys. Res., 102, 16663–16682, https://doi.org/10.1029/97JD00237, 1997.

Raymond, D. J.: The Hadley circulation as a radiative–convective instability, J. Atmos. Sci., 57, 1286-1297., https://doi.org/10.1175/1520-0469(2000)057<1286:THCAAR>2.0.CO;2, 2000.

Rind, D., and Rossow, W. B.: The effects of physical processes on the Hadley circulation, J. Atmos. Sci., 41, 479-507, https://doi.org/10.1175/1520-0469(1984)041<0479:TEOPPO>2.0.CO;2, 1984.

https://doi.org/10.5194/egusphere-2026-5049
Preprint. Discussion started: 11 September 2026

Sepulveda Araya, E. I., Sullivan, S. C., and Voigt, A.: Ice crystal complexity leads to weaker ice cloud radiative heating in idealized single-column simulations, Atmos. Chem. Phys., 25, 8943–8958, https://doi.org/10.5194/acp-25-8943-2025, 2025.

Slingo, J. M., and Slingo, A.: The response of a general circulation model to cloud longwave radiative forcing. II: Further studies, Quart. J. Roy. Meteor. Soc., 117, 333–364, https://doi.org/10.1002/qj.49711749805, 1991.

Sokol, A. B., Wall, C. J., and Hartmann, D. L: Greater Climate Sensitivity Implied by Anvil Cloud Thinning, Nature Geoscience, 17, 398–403, https://doi.org/10.1038/s41561-024-01420-6, 2024.

Stephens, G. L.: The parameterization of radiation for numerical weather prediction and climate models, Month. Weather Rev., 112, 826-867, https://doi.org/10.1175/1520-0493(1984)112<0826:TPORFN>2.0.CO;2, 1984.

Stubenrauch, C. J., Feofilov, A. G., Protopapadaki, S. E., and Armante, R.: Cloud Climatologies from the Infrared Sounders AIRS and IASI: Strengths and Applications, Atmos. Chem. Phys., 17, 13625–13644, https://doi.org/10.5194/acp-17-13625-2017, 2017.

Stubenrauch, C. J., Bonazzola, M., Protopapadaki, S. E., and Musat, I.: New Cloud System Metrics to Assess Bulk Ice Cloud Schemes in a GCM, J. Advances in Modeling Earth Systems, 11, 3212–3234, https://doi.org/10.1029/2019MS001642, 2019.

Stubenrauch, C. J., Caria, G., Protopapadaki, S. E., and Hemmer, F.: 3D Radiative Heating of Tropical Upper Tropospheric Cloud Systems Derived from Synergistic A-Train Observations and Machine Learning, Atmos. Chem. Phys., 21, 1015–1034, https://doi.org/10.5194/acp-21-1015-2021, 2021.

Stubenrauch, C. J., Kinne, S., Mandorli, G., Rossow, W., Winker, D., Ackerman, S., Chepfer, H., Girolamo, L., Garnier, A., Heidinger, A., K.-G, K., Meyer, K., Minnis, P., Platnick, S., Stengel, M., Sun-Mack, S., Veglio, P., Walther, A., Cai, X., and Zhao, G.: Lessons Learned from the Updated GEWEX Cloud Assessment Database, Surv. Geophys., 45, 1999–2048, https://doi.org/10.1007/s10712-024-09824-0, 2024.

Vallis, G. K., Zurita-Gotor, P., Cairns, C., and Kidston, J.: Response of the large-scale structure of the atmosphere to global warming, Quart. J. Royal Meteorol. Soc., 141, 1479-1501, https://doi.org/10.1002/qj.2456, 2015.

Voigt, A., and Albern, N.: No Cookie for climate change, Geophys. Res. Lett., 46, 14751–14761, https://doi.org/10.1029/2019GL084987, 2019.

Voigt, A., Bony, S., Dufresne, J. L., and Stevens, B.: The radiative impact of clouds on the shift of the intertropical convergence zone, Geophys. Res. Lett., 41, 4308-4315, https://doi.org/10.1002/2014GL060354, 2014.

Voigt, A., North, S., Gasparini, B., and Ham, S.-H.: Atmospheric cloud-radiative heating in CMIP6 and observations and its response to surface warming, Atmos. Chem. Phys., 24, 9749–9775, https://doi.org/10.5194/acp-24-9749-2024, 2024.

Zhao, M.: An Investigation of the Connections among Convection, Clouds, and Climate Sensitivity in a Global Climate Model, J. Climate, 27, 1845–1862, https://doi.org/10.1175/JCLI-D-13-00145.1, 2014.